

# Internal photoemission from plasmonic nanoparticles: comparison between surface and volume photoelectric effects

Cite this: *Nanoscale*, 2014, 6, 4716

Alexander V. Uskov,<sup>\*abcd</sup> Igor E. Protsenko,<sup>ab</sup> Renat S. Ikhsanov,<sup>e</sup>  
Viktoria E. Babicheva,<sup>fg</sup> Sergei V. Zhukovsky,<sup>fg</sup> Andrei V. Lavrinenko,<sup>f</sup> Eoin P. O'Reilly<sup>h</sup>  
and Hongxing Xu<sup>cd</sup>

We study the emission of photoelectrons from plasmonic nanoparticles into a surrounding matrix. We consider two mechanisms of electron emission from the nanoparticles – surface and volume ones – and use models for these two mechanisms which allow us to obtain analytical results for the photoelectron emission rate from a nanoparticle. Calculations have been carried out for a step potential at the surface of a spherical nanoparticle, and a simple model for the hot electron cooling has been used. We highlight the effect of the discontinuity of the dielectric permittivity at the nanoparticle boundary in the surface mechanism, which leads to a substantial (by ~5 times) increase of the internal photoelectron emission rate from a nanoparticle compared to the case when such a discontinuity is absent. For a plasmonic nanoparticle, a comparison of the two photoeffect mechanisms was undertaken for the first time which showed that the surface photoeffect can in the general case be larger than the volume one, which agrees with the results obtained for a flat metal surface first formulated by Tamm and Schubin in their pioneering development of a quantum-mechanical theory of photoeffect in 1931. In accordance with our calculations, this possible predominance of the surface effect is based on two factors: (i) effective cooling of hot carriers during their propagation from the volume of the nanoparticle to its surface in the scenario of the volume mechanism and (ii) strengthening of the surface mechanism through the effect of the discontinuity of the dielectric permittivity at the nanoparticle boundary. The latter is stronger at relatively lower photon energies and correspondingly is more substantial for internal photoemission than for an external one. We show that in the general case, it is essential to take both mechanisms into account in the development of devices based on the photoelectric effect and when considering hot electron emission from a plasmonic nanoantenna.

Received 17th December 2013  
Accepted 11th February 2014

DOI: 10.1039/c3nr06679g

www.rsc.org/nanoscale

## 1 Introduction

A recent publication by Chalabi and Brongersma<sup>1</sup> was entitled “Harvest season for hot electrons”, and this title excellently

illustrates a boom of interest in the generation of hot photoelectrons in plasmonic nanostructures which is occurring at present. Indeed, the enhanced photoelectron emission from single plasmonic nanoantennas and from ensembles of such nanoantennas is under intensive study for application in Schottky barrier photodetectors in order to achieve higher device sensitivity;<sup>2–14</sup> in solar cells with the goal to enhance their photovoltaic efficiency by harvesting solar photons below the semiconductor bandgap energy;<sup>2,4,6,11,14–21</sup> in (nano-)photoelectrochemistry and (nano-)photochemistry,<sup>2,4,22–30</sup> including, in particular, water splitting;<sup>25,26,28–30</sup> for the realization of new photoconductive plasmonic metamaterials;<sup>6</sup> and in molecular electronics<sup>31</sup> – *i.e.* in all areas of science and technology where the generation of hot photoelectrons and their subsequent utilization play a principal role. In addition, the emission of hot electrons can enhance the characteristics of solar concentrator systems.<sup>32</sup> Developments and proposals based on the use of the emission of photoelectrons from plasmonic nanoantennas

<sup>a</sup>P. N. Lebedev Physical Institute, Russian Academy of Sciences, Leninsky pr. 53, 119991 Moscow, Russia. E-mail: alexusk@lebedev.ru; Fax: +7-495-9382251; Tel: +7-499-1326139

<sup>b</sup>Advanced Energy Technologies Ltd, Skolkovo, Novaya ul. 100, 143025, Moscow Region, Russia

<sup>c</sup>School of Physics & Technology, Wuhan University, Wuhan, 430072, P. R. China

<sup>d</sup>Institute of Physics, Chinese of Academy of Sciences, P. O. Box 603-146, Beijing, 100190, P. R. China

<sup>e</sup>Research Institute of Scientific Instruments, State Nuclear Energy Corporation “Rosatom”, Moscow, Russia

<sup>f</sup>DTU Fotonik, Technical University of Denmark, Ørstedts Plads 343, DK-2800 Kgs., Lyngby, Denmark

<sup>g</sup>National Research University for Information Technology, Mechanics, and Optics, Kronverkskiy, 49, St. Petersburg 197101, Russia

<sup>h</sup>Tyndall National Institute, Cork, Ireland

(nanotips, first of all) into vacuum – including novel nanometer-sized femtosecond electron sources,<sup>33</sup> femtosecond photoelectron emission spectroscopy,<sup>34</sup> and the attosecond nanoplasmonic-field microscopy are also worth noting.<sup>35</sup>

Obviously, understanding the physical mechanisms that result in the emission of photoelectrons from plasmonic nanoparticles and nanostructures is essential for the development of devices based on this phenomenon. Research on this topic dates back to the pioneering work on a quantum-mechanical theory of the photoelectric effect from metals written in 1931 by Tamm and Schubin,<sup>36</sup> who introduced and described two mechanisms contributing to the effect – see Fig. 1.

(A) A surface mechanism (or the surface photoelectric effect, see Fig. 1a), in which an electron absorbs a photon during its collision with the metal surface (boundary) and, if the energy received by the electron is sufficient to overcome the potential barrier at the boundary (Schottky barrier if the metal is in contact with a semiconductor), then the electron is emitted from the metal into the matrix surrounding the metal (semiconductor, for instance) during this inelastic collision with the metal surface. In this case, the electron also can be reflected back into the metal after photon absorption during the collision.<sup>37</sup> In the surface mechanism for the photoeffect, the rate of photoelectron emission from the metal is proportional to the square of the electromagnetic field component normal to the metal surface<sup>36</sup> – see below.

(B) A volume (or bulk) mechanism (or the volume photoelectric effect, see Fig. 1b), which consists of three phases (see ref. 38 for a comprehensive review primarily devoted to this bulk mechanism).

(1) An electron absorbs a photon inside the metal during its collision with an impurity, phonon, lattice defect, *etc.*<sup>39</sup> or due to its coupling to the periodic lattice potential<sup>36,40</sup> and becomes “hot”;

(2) then the electron moves to the boundary of the metal (this “electron transport” phase is absent in the surface mechanism), colliding with phonons and cold electrons and losing energy in the process;

(3) if the electron reaches the metal surface with energy that is still sufficient to overcome the potential barrier at the boundary of the metal, the electron may be emitted into the matrix (semiconductor) surrounding the metal.

Obviously, the photoelectron emission rate from the metal in the scenario of the bulk photoeffect is proportional to the light absorption coefficient of the bulk metal; it depends on the energy distribution of hot electrons after their generation and also on the cooling rate of electrons during their motion to the nanoparticle boundary.

Having identified and compared these two mechanisms, Tamm and Schubin in ref. 36 considered mechanism (A) as dominating in the visible and IR ranges. Nevertheless, for several decades after the publication of ref. 36, researchers returned to the discussion on the above mechanisms for photoelectron emission from a metal (see ref. 38 and 41–50 and references therein), and in particular, to the arguments as to which of the two mechanisms is more important. The main argument against the surface mechanism (A) in those discussions was that the component of field normal to the surface (to the square of which the photoelectron emission rate in the surface mechanism is proportional) is absent if light is incident normally on a flat metal surface, as was relevant in many practical cases. However, it became clear in the 1960s and 70s (see ref. 46–50 and references therein) that the roughness of a metal surface can lead to the appearance of a normal component to the metal surface (in particular, due to the conversion of an incident plane wave into a surface plasmonic wave<sup>49</sup>), so that mechanism (A) can be essential even for macroscopically flat structures with normal incidence of light.

Nevertheless, the question as to which of the two mechanisms of photoelectron emission is dominant has been left open until the present time, with various groups adopting different approaches. Several years ago, Berini with his co-authors used the volume mechanism (B) as the basis for their consideration of thin-film Schottky barrier photodetectors,<sup>7–9</sup> and very recently Halas and Nordlander with their colleagues<sup>3,12,13</sup> have used the description of the volume mechanism given in ref. 7 to analyze the emission of photoelectrons from plasmonic nanoantennas. On the other hand, the theory of photoelectron emission from metallic nanoparticles developed in ref. 6 and then used in calculations in ref. 11 and 14 is based primarily on the surface mechanism (A). In ref. 51 Govorov and co-authors developed an approach to the theory of photoelectron emission from a plasmonic nanoparticle starting from a quantum microscopic description of the non-equilibrium carrier population in a localized plasmon wave. As nanostructures of more and more intricate shapes are introduced, the discussion on a proper description of photoelectron emission from metals in general and from metal nanostructures in particular is again of current importance.

In this paper, we compare the surface and volume mechanisms of internal photoelectron emission from plasmonic nanoparticles. Using spherical particles as a simple and analytically tractable example, we derive comparable metrics for each of the two mechanisms. Comparing these metrics, we conclude that the volume mechanism could only prevail if hot

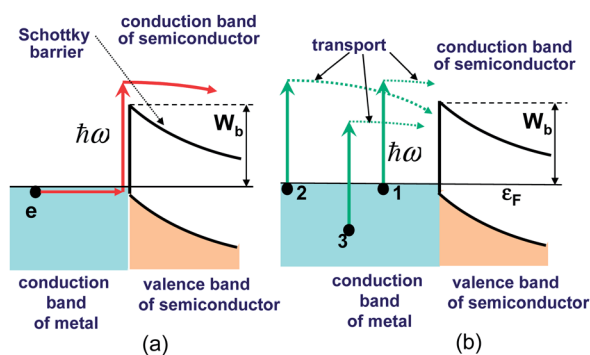


Fig. 1 Illustration of the two mechanisms of the photoelectric effect. (a) Surface effect: an electron collides with the Schottky barrier, absorbs the photon energy  $\hbar\omega$ , and leaves the metal. (b) Volume effect: electron 1 receives energy  $\hbar\omega$ , moves to the Schottky barrier, and overcomes it, leaving the metal; electrons 2 and 3 do not have sufficient energy when they reach the barrier and remain in the metal.  $W_b$  is the work function of the metal to semiconductor;  $\epsilon_F$  is the Fermi level.

electrons were able to reach the nanoparticle surface without energy loss. In realistic cases, the “cooling” processes during “hot” electron transport often lead to the prevalence of the surface photoelectric effect, especially for smaller nanoparticles and lower photon energies.

The paper is organized as follows. In Section II we provide a detailed account on the theory of internal photoelectron emission from plasmonic nanoparticles. In particular, in Section II-A, the problem is formulated, and the concept of the cross-section of photoelectron emission from a nanoparticle is introduced. In Section II-B, formulae are presented to calculate the internal photoelectron emission rate from a nanoparticle and the photoelectron emission cross-section of a spherical nanoparticle for the surface photoelectric effect, based on the work in ref. 6 and using a simple model with a step potential at the nanoparticle boundary. In Section II-C, a model is presented to calculate the internal quantum efficiency for the volume photoelectric mechanism of photoeffect, including the derivation of an expression for the photoelectron emission cross-section for the volume mechanism. In Section III, numerical results are presented to compare the two mechanisms, and the basic assumptions of the calculations are discussed in detail. Finally, Section IV formulates the conclusions.

## II Theory of the photoelectric effect

### A Formulation of the problem

The following problem is under consideration – see Fig. 2. A plane light wave of frequency  $\omega$  and with intensity  $S$  propagates along the  $z'$ -axis in a background matrix (dielectric or semiconductor) with relative permittivity  $\epsilon_e$ . The amplitude  $\mathbf{E}_o$  of the electric field of the light is polarized along the  $y'$  direction. The wave is incident on an imbedded metal nanoparticle with relative permittivity  $\epsilon_i(\omega)$ . For simplicity, we consider a spherical nanoparticle with radius  $a$  so that in the quasistatic approximation<sup>52</sup> the field  $\mathbf{E}_i$  inside the nanoparticle is homogeneous, parallel to  $\mathbf{E}_o$  and can be expressed as:<sup>52</sup>

$$\mathbf{E}_i = \frac{3\epsilon_e}{\epsilon_i(\omega) + 2\epsilon_e} \mathbf{E}_o \equiv F \cdot \mathbf{E}_o \quad (1)$$

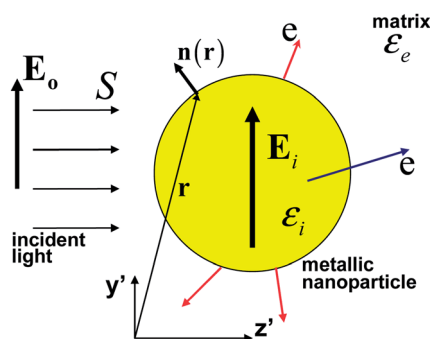


Fig. 2 Schematic illustration of a spherical metallic nanoparticle (with permittivity  $\epsilon_i$ ) imbedded in a dielectric (or semiconductor) matrix (with permittivity  $\epsilon_e$ ). The incident plane wave with an electrical field  $\mathbf{E}_o$  causes an electric field  $\mathbf{E}_i$  inside the nanoparticle. Red arrows illustrate the surface photoelectric mechanism, while the blue arrow shows the volume (bulk) photoelectric mechanism.

When the light frequency  $\omega$  approaches the localized plasmonic frequency  $\omega_{\text{LPR}}$  which satisfies the Fröhlich conditions<sup>52</sup>

$$\text{Re}[\epsilon_i(\omega_{\text{LPR}})] + 2\epsilon_e = 0 \quad (1a)$$

then, as one can see from (1), a resonant enhancement of the field takes place (the localized plasmonic resonance). One should stress that the quasistatic approximation makes the resonance frequency  $\omega_{\text{LPR}}$  independent of the nanoparticle size, and the increase of  $\epsilon_e$  lowers  $\omega_{\text{LPR}}$  approximately as  $\sim 1/\sqrt{1+2\epsilon_e}$ . Note that the homogeneous field assumption may be violated in the presence of a strong plasmonic resonance and/or for nanoparticles of more complex shapes (e.g., nanoantennas), where strong field localization effects can lead to field inhomogeneity inside the nanoparticle. However, the presented formalism is straightforwardly generalized to the case of an inhomogeneous field, albeit at the cost of no longer being analytically tractable.

The electrons in the metal absorb photons with energy  $\hbar\omega$  (A) during their collisions with the nanoparticle surface (surface photon absorption) and (B) inside the nanoparticle (volume photon absorption)<sup>36,37</sup> and can leave the nanoparticle in either case. For the volume mechanism, our model is limited by the case when the imaginary part  $\epsilon_i''(\omega)$  of the metal permittivity  $\epsilon_i(\omega)$  includes only the contribution of free electrons, but not contributions from interband transitions in metal. Therefore, it is applicable only for  $\hbar\omega \leq 1.9$  eV (for gold) and for higher energies, the contribution of interband transitions becomes important.<sup>52</sup>

Our goal is to calculate and to compare the photoelectron emission rates from the nanoparticle due to the surface and the volume absorption of photons. In the next two subsections, we present separately our calculations for the surface and volume (bulk) photoelectric effects from a metal nanoparticle.

The ability of plasmonic nanoparticles to emit photoelectrons can be characterized by the photoelectron emission cross-section of the nanoparticle.<sup>6</sup> Namely, the photoelectron emission cross-section is:

$$\sigma_{\text{em}} = R_{\text{em}}/(S/\hbar\omega) \quad (2)$$

where  $R_{\text{em}}$  is the rate of emission of photoelectrons from the nanoparticle in (1/s), and  $S/\hbar\omega$  is the photon flux [in  $1/(\text{m}^2 \text{ s})$ ] incident on the nanoparticle. Below we calculate  $R_{\text{em}}$  and  $\sigma_{\text{em}}$  for both the surface and volume photoelectric effects.

### B Theory of the surface photoelectric effect

In this subsection, we briefly introduce the theory of the surface mechanism for photoelectron emission, following the approach used in ref. 6 where the theory is presented in more detail. If the de Broglie electron wavelength  $\lambda$  in the metal is much smaller than the characteristic nanoparticle size  $L_{\text{nano}}$ ,  $\lambda \ll L_{\text{nano}}$  (one should note that in silver and gold  $\lambda \approx 0.5$  nm), then we can safely neglect quantum-confinement effects in the metal. In other words, the electron gas is uniformly distributed with an equilibrium density given by that of the bulk metal. Furthermore, we can calculate the rate  $u(\mathbf{r})$  of electron emission per unit

area of the nanoparticle surface [ $1/(\text{s m}^2)$ ], by considering the nanoparticle surface at the coordinate  $\mathbf{r}$  (see Fig. 2) as being flat and by using the theory of photoelectron emission due to collisions of metal electrons with a flat boundary. Within this approximation, the rate  $u(\mathbf{r})$  is proportional to the square of the normal component  $E_1^{(n)}(\mathbf{r}) = \mathbf{n}(\mathbf{r}) \cdot \mathbf{E}_1$  of the field  $\mathbf{E}_1$ .<sup>6,36,41–43</sup>

$$u(\mathbf{r}) = C_{\text{em}}^{\text{surface}} \cdot |E_1^{(n)}(\mathbf{r})|^2 \quad (3)$$

where  $\mathbf{n}(\mathbf{r})$  is the unit vector normal to the nanoparticle surface. The coefficient  $C_{\text{em}}^{\text{surface}}$  is calculated quantum-mechanically (see below) and depends, in particular, on the electron density in the metal, on the photon energy  $\hbar\omega$ , on the potential barrier for electrons at the nanoparticle boundary, and on any discontinuities in the permittivity and the electron mass at the interface between the metal and the surrounding matrix. Correspondingly, the photoelectron emission rate due to electron collisions with the total nanoparticle surface is:

$$R_{\text{em}}^{\text{surface}} = \int_{\text{surface}} dS u(\mathbf{r}) = C_{\text{em}}^{\text{surface}} \int_{\text{surface}} dS |E_1^{(n)}(\mathbf{r})|^2 \quad (4)$$

where the integral extends over the entire nanoparticle surface. Since the field inside a spherical nanoparticle is homogeneous, we get easily:

$$R_{\text{em}}^{\text{surface}} = C_{\text{em}}^{\text{surface}} \cdot A_{\text{nano}} |\mathbf{E}_1|^2 / 3 \quad (5)$$

where  $A_{\text{nano}} = 4\pi a^2$  is the area of the nanoparticle surface.

The coefficient  $C_{\text{em}}^{\text{surface}}$  in (2) can be found by solving the quantum-mechanical problem for the collision of a single electron with a metal boundary, and then subsequently summing over all metal electrons undergoing such collisions with the surface. Fig. 3 illustrates this problem. The metal boundary is modelled by the 1D potential barrier  $U(z)$  where the axis  $z$  is normal to the boundary and, in this section, we perform

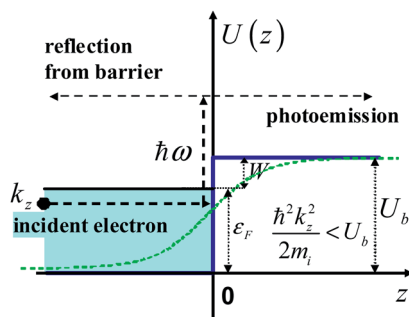


Fig. 3 Schematic illustration of inelastic scattering of an electron at a metal boundary in the presence of an optical field. The potential energy profile  $U(z)$  is plotted along the direction  $z$  normal to the metal boundary. An electron incident on the boundary (wave vector  $k_z$ ) scatters inelastically, by absorption of a photon (energy  $\hbar\omega$ ). In the collision with the boundary, the electron can be partly back-reflected into the metal or be forward scattered into the dielectric matrix (photoelectron emission). The blue line is a step potential with height  $U_b = \varepsilon_F + W$  where  $\varepsilon_F$  is the Fermi energy in the metal;  $W$  is the work function; the green curve illustrates an example of a gradually changing potential  $U(z)$ .

the calculation for an abruptly changing (at  $z = 0$ ) potential (a step potential) with a step of height  $U_b$ , as indicated in Fig. 3. The potential step  $U_b$  can be written as  $U_b = \varepsilon_F + W_b$  where  $\varepsilon_F$  is the Fermi energy in the metal, and  $W_b$  is the work function of the metal, bordering the surrounding medium. The electron masses in the metal  $m_i$  and in the surrounding medium (barrier)  $m_e$  can be different from each other, in general. We consider an electron plane wave in the metal incident on the metal boundary with wave vector  $\mathbf{k}_i = (k_{ix}, k_{iy}, k_{iz})$ . In the absence of an electromagnetic field, electron scattering from the barrier is elastic and furthermore the parallel wave vector component is conserved (since the surface is assumed to be locally flat). On the other hand, the electron may scatter inelastically in the presence of an electromagnetic field, *i.e.* by absorbing a photon with energy  $\hbar\omega$ . While the parallel momentum of the electron is still conserved (neglecting the vanishing momentum of the photon itself), it may either scatter back into the metal or out into the surrounding matrix – see Fig. 3. We denote the corresponding probabilities by  $p_{\text{in}}$  and  $p_{\text{out}}$ , respectively. Both probabilities  $p_{\text{in}}$  and  $p_{\text{out}}$  are proportional to the square of the normal component  $E_1^{(n)}(\mathbf{r})$  of the field  $\mathbf{E}_1$  in the metal.<sup>6,36,41–45</sup>

$$p_{\text{in}} = c_{\text{in}} \cdot |E_1^{(n)}(\mathbf{r})|^2 \quad (6)$$

$$p_{\text{out}} = c_{\text{out}} \cdot |E_1^{(n)}(\mathbf{r})|^2 \quad (7)$$

Note that the normal component  $E_1^{(n)}$  inside the metal is related to the normal component  $E_e^{(n)}$  in the surrounding medium by:

$$\varepsilon_i E_1^{(n)} = \varepsilon_e E_e^{(n)} \quad (8)$$

We concentrate below on the calculation of the photoelectron emission probability  $p_{\text{out}}$ . Obviously, with a step potential as in Fig. 3, the photoelectron emission from the metal can occur (*i.e.*,  $c_{\text{out}} > 0$ ) only if the electron gains sufficient energy to overcome the barrier, *i.e.* only if  $\hbar^2 k_{iz}^2 / (2m_i) + \hbar\omega > U_b$ .

Although the probability  $p_{\text{out}}$  can be calculated using various quantum-mechanical methods, it was found in ref. 6 through direct solution of the Schrödinger equation for an electron in the presence of the field using perturbation theory (see also a very detailed description in ref. 41). In this solution, the electron wave function in the barrier far from the boundary ( $z \rightarrow \infty$ ) contains the component:

$$C_+(\infty) \cdot \exp \left[ -i \frac{\varepsilon(\mathbf{k}_i) + \hbar\omega}{\hbar} t + i(k_{ix}x + k_{iy}y + k_{ez}^+ z) \right] \quad (9)$$

describing an electron of initial energy in the metal

$$\varepsilon(\mathbf{k}_i) = \hbar^2 (k_{ix}^2 + k_{iy}^2 + k_{iz}^2) / (2m_i) \quad (10)$$

which absorbed a photon of energy  $\hbar\omega$  and left the metal for the surrounding medium. The  $z$ -component  $k_{ez}^+$  of the electron wave vector after the electron is emitted outside the metal after absorption of the photon is determined from the energy conservation law:

$$\frac{\hbar^2(k_{ix}^2 + k_{iy}^2 + k_{iz}^2)}{2m_i} + \hbar\omega = \frac{\hbar^2[k_{ix}^2 + k_{iy}^2 + (k_{ez}^+)^2]}{2m_e} + U_b \quad (11)$$

The amplitude  $C_+(\infty)$  is proportional to the normal component  $E_i^{(n)}$  of the field in the metal and can be written as

$$C_+(\infty) = (b_V U_b + b_m \Delta m + b_e \Delta \varepsilon) E_i^{(n)} \quad (12)$$

where  $\Delta m = m_e - m_i$  and  $\Delta \varepsilon = \varepsilon_e - \varepsilon_i$ ; and  $b_V$ ,  $b_m$ , and  $b_e$  are some coefficients, which are in general complex numbers. The emission probability  $p_{\text{out}}$  is expressed through the amplitude  $C_+(\infty)$  as:

$$p_{\text{out}} = \frac{\text{Re}[k_{ez}^+]}{k_{iz}} |C_+(\infty)|^2 \quad (13)$$

where we assume the unit probability amplitude for the electron plane wave wavefunction incident from the metal to the barrier. Correspondingly,

$$c_{\text{out}} = \frac{k_{ez}^+}{k_{iz}} |b_V U_b + b_m \Delta m + b_e \Delta \varepsilon|^2 \quad (14)$$

Eqn (14) demonstrates clearly that photon absorption by an electron with emission from the metal takes place due to (a) the jump  $U_b$  in the potential, (b) the discontinuity  $\Delta m$  of the electron mass, and (c) the discontinuity  $\Delta \varepsilon$  of the dielectric constant at the nanoparticle surface. Photon absorption due to a nonzero  $\Delta \varepsilon$  can be considered as the inverse to the transit radiation effect, where an electron crosses the boundary between two media with different dielectric constants and emits light.<sup>53</sup> Below, we show that nonzero  $\Delta \varepsilon$  substantially increases the surface photoelectric effect.

We assume for simplicity that  $\Delta m = 0$ , so that  $m_e = m_i \equiv m$ . In this case, calculating the coefficients  $b_V$  and  $b_e$  as in ref. 6, we derive the formula:

$$c_{\text{out}} = \frac{8e^2 U_b}{m \hbar^2 \omega^4} \cdot \text{Re} \left[ \sqrt{\left( X - 1 + \frac{\hbar\omega}{U_b} \right)} \right] \cdot \frac{G(X)}{\sqrt{X}} \cdot |K_{\Delta \varepsilon}(X)|^2 \quad (15)$$

where  $e$  is the electron charge,  $X = \varepsilon_{iz}(k_{iz})/U_b$  with  $\varepsilon_{iz}(k_{iz}) = \hbar^2 k_{iz}^2 / (2m)$  so that the coefficient  $c_{\text{out}}$  depends only on the  $z$ -component  $k_{iz}$  of the initial vector  $\mathbf{k}_i$ , normal to the boundary:  $c_{\text{out}} = c_{\text{out}}[\varepsilon_{iz}(k_{iz})]$ ;

$$G(X) = X \cdot \frac{|\sqrt{X} - \sqrt{X-1}|^2}{|\sqrt{X + \hbar\omega/U_b} + \sqrt{X + \hbar\omega/U_b - 1}|^2} \quad (16)$$

and the coefficient

$$K_{\Delta \varepsilon} = \frac{1}{2} \left[ \left( \frac{\varepsilon_i}{\varepsilon_e} + 1 \right) - \left( \frac{\varepsilon_i}{\varepsilon_e} - 1 \right) \left( \sqrt{X + \frac{\hbar\omega}{U_b}} + \sqrt{X-1} \right)^2 \right] \quad (17)$$

describes the effect of the discontinuity  $\Delta \varepsilon$  on the photon absorption and photoelectron emission – if  $\varepsilon_e = \varepsilon_i$ , we have  $K_{\Delta \varepsilon} \equiv 1$ .

Summing over all electrons in the metal that collide with the surface in the metal, one can obtain the coefficient in eqn (3) as:

$$C_{\text{em}}^{\text{surface}} = \int_{k_{iz} > 0} \frac{2d\mathbf{k}_i}{(2\pi)^3} f_{\text{F}}(\mathbf{k}_i) \cdot v_{iz} \cdot c_{\text{out}} \quad (18)$$

where  $f_{\text{F}}(\mathbf{k}_i) = \{1 + \exp[(\varepsilon(\mathbf{k}_i) - \varepsilon_{\text{F}})/k_{\text{B}}T_e]\}^{-1}$  is the Fermi–Dirac equilibrium distribution function of electrons in the metal,  $T_e$  is the electron temperature, and  $v_{iz} = \hbar k_{iz}/m$  is the electron velocity component normal to the metal boundary. Since the coefficient  $c_{\text{out}}$  depends only on  $k_{iz}$  (not on  $k_{ix}$  and  $k_{iy}$ ), the 3D integrals in (18) can be easily converted into 1D-integrals over  $k_{iz}$ .

Let us introduce the dimensionless coefficient  $\eta_o$  related to  $C_{\text{em}}^{\text{surface}}$  as:<sup>6</sup>

$$\eta_o = \frac{\hbar\omega}{2\varepsilon_o c} \cdot C_{\text{em}}^{\text{surface}} \quad (19)$$

through which the external quantum efficiency (the quantum yield) for devices based on photoelectron emission from ensembles of nanoantennas can be expressed.<sup>11,14</sup> The parameter  $\eta_o$  itself can be interpreted as the external quantum efficiency of a device in which the incident light with intensity  $S_{\text{vac}} = 2\varepsilon_o c |E_{\text{vac}}|^2$  in vacuum ( $E_{\text{vac}}$  is the electric field of light) creates the normal component  $E_i^{(n)} = E_{\text{vac}}$ . Correspondingly, from eqn (15), (18) and (19) we have for  $T_e = 0$ :

$$\eta_o = \frac{8}{\pi} \alpha_{\text{F-s}} \cdot \left( \frac{U_b}{\hbar\omega} \right)^3 \cdot \int_{1-\hbar\omega/U_b}^{\varepsilon_{\text{F}}/U_b} dX \text{Re} \left[ \sqrt{\left( X - 1 + \frac{\hbar\omega}{U_b} \right)} \right] \times \frac{G(X)}{\sqrt{X}} |K_{\Delta \varepsilon}(X)|^2 \left( \frac{\varepsilon_{\text{F}}}{U_b} - X \right) \quad (20)$$

where  $\alpha_{\text{F-s}} = e^2/(4\pi\varepsilon_o \hbar c) = 0.007297 \sim 1/137$  is the fine-structure constant, and we assume that  $\hbar\omega < \varepsilon_{\text{F}}$ . The blue curve in Fig. 4 illustrates the dependence of  $\eta_o$  on the photon energy  $\hbar\omega$ . In our calculations, we assumed that a gold nanoparticle is surrounded with a medium with  $\varepsilon_e = 13$  (like GaAs). For gold, we used the dielectric constant  $\varepsilon_i(\omega)$  from ref. 54. Correspondingly, [see condition (1a)], the plasmonic resonance in a spherical nanoparticle occurs at  $\hbar\omega_{\text{pr}} = 1.48$  eV (we reiterate that in the quasistatic approximation used here the frequency  $\omega_{\text{pr}}$  does not

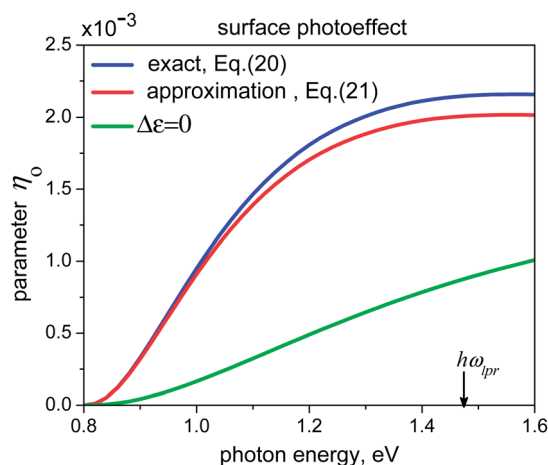


Fig. 4 Spectral dependence of the photoelectron emission parameter  $\eta_o = \eta_o(\hbar\omega)$ . The blue curve is calculated from eqn (20), the red one is the approximation (21). The green curve is obtained by assuming  $\Delta \varepsilon = 0$  [i.e.,  $K_{\Delta \varepsilon}(X) \equiv 1$  in eqn (20)].  $\hbar\omega_{\text{pr}}$  is the photon energy where the plasmonic resonance occurs in the nanoparticle.

depend on the radius  $a$ ). We also used the values  $\varepsilon_F = 5.51$  eV and  $W_b = 0.8$  eV. One can see that the parameter  $\eta_o$  changes from zero at the threshold ( $\hbar\omega = 0.8$  eV) to  $\sim 0.002$  at  $\hbar\omega \sim 1.6$  eV. The red curve illustrates eqn (21) obtained from (20) by approximate integration:

$$\eta_o \approx \frac{32\alpha_{s-f}}{15\pi} \left(\frac{U_b}{\hbar\omega}\right)^3 \sqrt{\frac{1}{\bar{X}}} G(\bar{X}) |K_{\text{dis}}(\bar{X})|^2 \left(\frac{\hbar\omega - W_b}{U_b}\right)^{5/2} \quad (21)$$

where  $\bar{X} = 0.5 [1 + (\varepsilon_F - \hbar\omega)/U_b]$ . Formula (21) shows clearly that, near the threshold, when the photon energy  $\hbar\omega$  approaches the work function  $W_b$ ,

$$\eta_o \propto (\hbar\omega - W_b)^{5/2} \quad (22)$$

Eqn (22) is different from the parabolic Fowler's law where  $\eta_o \propto (\hbar\omega - W_b)^2$  (ref. 55) and is found, in general, when the potential  $U(z)$  at the metal boundary changes sharply rather than gradually. In contrast, the parabolic Fowler's law works well for gradually changing potentials (see for example the green curve in Fig. 3; see also ref. 43–45, for instance).

The green curve in Fig. 4 shows the parameter  $\eta_o$  when  $\Delta\varepsilon = 0$  [i.e.,  $K_{\Delta\varepsilon}(\bar{X}) \equiv 1$  in eqn (20)]. A comparison of the blue and green curves demonstrates that a nonzero discontinuity  $\Delta\varepsilon$  of the dielectric constant  $\varepsilon$  at the boundary between the metal and surrounding medium substantially (by 3–10 times) increases the surface photoelectron emission parameter  $\eta_o$ .

The blue and green curves in Fig. 4 show also that the initial fast growth of  $\eta_o$  saturates with increasing photon energy  $\hbar\omega$  and, after this saturation, the parameter  $\eta_o$  decreases (not shown). This behaviour is due to the strong suppression of the interaction of an electron with the electromagnetic field with increasing photon energies  $\hbar\omega$  – see the  $1/\omega^4$  dependence in eqn (15). This circumstance, in particular, leads to a diminished role of the surface mechanism compared to the bulk mechanism with increasing photon energy  $\hbar\omega$  – see Section III.

Following the definition of (2) and using (5) and (19), we can obtain a formula for the photoelectron emission cross-section due to the surface photoelectric effect:

$$\sigma_{\text{em}}^{\text{surface}} = \frac{4\pi\eta_o}{3\varepsilon_e^{1/2}} |F|^2 \cdot a^2 \quad (23)$$

where we have used the expression  $S = 2\varepsilon_o\varepsilon_e^{1/2}c|\mathbf{E}_o|^2$ . The enhancement of the photoelectron emission cross-section due to plasmonic nanoantenna effects is included in eqn (23) through the factor  $|F|^2$  (see also eqn (1)). Examples of the calculation of  $\sigma_{\text{em}}^{\text{surface}}$  can be found in ref. 6.

### C Calculation of the volume photoelectric effect

In our modeling of the volume photoelectric effect from a metal nanoparticle we follow closely the approach taken by Chen and Bates<sup>56</sup> (see also the three-step description of the volume mechanism in ref. 38 and 57, and references therein). The power absorbed inside the nanoparticle is given by:<sup>52</sup>

$$P = 2\omega\varepsilon_o\varepsilon_i'' \int_{\text{volume}} \mathbf{dr} \cdot |\mathbf{E}_i|^2 = 2\omega\varepsilon_o\varepsilon_i'' \cdot |\mathbf{E}_i|^2 V_{\text{nano}} \quad (24)$$

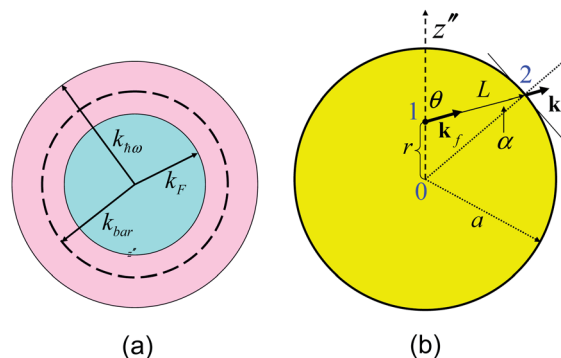


Fig. 5 (a) Distribution of electrons in  $k$ -space. The blue colour shows the volume in  $k$ -space occupied by unexcited (cold) electrons; the pink colour illustrates excited (hot) electrons after photon absorption. Hot electrons outside the dashed line can be emitted from the nanoparticle. (b) Illustration of propagation of a hot electron in a spherical nanoparticle of radius  $a$ . A hot electron is generated at point 1 at a distance  $r$  from the centre  $O$  with wave vector  $\mathbf{k}_f$  and with angle  $\theta$  to the axis  $z''$ . In the absence of collisions, the electron moves along a straight line parallel to  $\mathbf{k}_f$  and collides with the nanoparticle surface at point 2.  $L$  is the length of the electron path before its collision with the nanoparticle boundary.  $\alpha$  is the incidence angle of the electron to the surface.  $\mathbf{k}_s$  is the wave vector of the electron as it collides with the surface.

where  $V_{\text{nano}} = 4\pi a^3/3$  is the nanoparticle volume. Correspondingly, the photon absorption rate (in 1/s) in the whole nanoparticle is:

$$R_{\text{abs}}^{\text{volume}} \equiv P/\hbar\omega = 2\hbar^{-1}\varepsilon_o\varepsilon_i'' \cdot |\mathbf{E}_i|^2 V_{\text{nano}} = r_{\text{abs}}^{\text{vol}} \cdot V_{\text{nano}} \quad (25)$$

where

$$r_{\text{abs}}^{\text{vol}} = 2\hbar^{-1}\varepsilon_o\varepsilon_i'' \cdot |\mathbf{E}_i|^2 \quad (26)$$

is the volume density for the photon absorption rate [1/(s m<sup>3</sup>)] in the nanoparticle. We assume that electrons in the metal before excitation by light have zero temperature,  $T_e = 0$ , so that cold electrons occupy the Fermi sphere in  $k$ -space with radius  $k_F = \sqrt{2m_i\varepsilon_F}/\hbar$ , see Fig. 5a. Then the excited (“hot”) electrons occupy a spherical layer above the Fermi sphere in  $k$ -space:

$$k_F = \sqrt{2m_i\varepsilon_F}/\hbar < k < k_{\text{ho}} = \sqrt{2m_i(\varepsilon_F + \hbar\omega)}/\hbar \quad (27)$$

(see Fig. 5a). If a hot electron, in its final state after photon absorption, has the energy  $E_f = \hbar^2 k_f^2/(2m_i)$  ( $\mathbf{k}_f$  is the wave vector of the hot electron) larger than the height  $U_b$  of the potential barrier, i.e.

$$E_f = \hbar^2 k_f^2/(2m_i) > U_b \equiv \hbar^2 k_{\text{bar}}^2/(2m_i) \quad (28)$$

(see Fig. 5a), then it has a chance to leave the nanoparticle. The ratio of the emission rate  $R_{\text{em}}^{\text{volume}}$  for hot electrons from the nanoparticle to the excitation rate for hot electrons inside the nanoparticle, which simply equals the photon absorption rate  $R_{\text{abs}}^{\text{volume}}$ , is, by definition, the internal quantum efficiency  $\eta_i$  of the volume photoelectric effect<sup>7</sup>,

$$\eta_i = R_{\text{em}}^{\text{volume}}/R_{\text{abs}}^{\text{volume}} \quad (29)$$

Below we calculate  $\eta_i$  for a spherical nanoparticle.

We assume in our calculations that the distribution of hot electrons in the layer in  $k$ -space is uniform and isotropic. This assumption is a key point in Fowler's statistical theory of photoelectric emission from metals;<sup>55</sup> we are adopting this assumption here (see also the modeling in ref. 7). Then, the density of the electron excitation rate in  $k$ -space, in units of  $\text{m}^3/(\text{s m}^3) = 1/\text{s}$ , is

$$r_{\text{exc}}^{(k)} = \frac{r_{\text{abs}}^{\text{vol}}}{V_{\text{layer}}^{(k)}} \quad (30)$$

where

$$V_{\text{layer}}^{(k)} = \frac{4\pi}{3} (k_{\text{hw}}^3 - k_{\text{F}}^3) \quad (31)$$

is the volume occupied in  $k$ -space by hot electrons.

If  $p_{\text{em}}(\mathbf{r}, \mathbf{k}_{\text{f}})$  is the probability of a hot electron (with wave vector  $\mathbf{k}_{\text{f}}$ , generated in the nanosphere at the position  $\mathbf{r}$ ) to be emitted from the nanoparticle, the photoelectron emission rate from the nanosphere is:

$$R_{\text{em}}^{\text{volume}} = \int_{\text{volume}} d\mathbf{r} \int_{\text{layer}} d\mathbf{k}_{\text{f}} r_{\text{exc}}^{(k)} \cdot p_{\text{em}}(\mathbf{r}, \mathbf{k}_{\text{f}}) = R_{\text{abs}}^{\text{volume}} \cdot \eta_{\text{i}} \quad (32)$$

where  $\eta_{\text{i}}$  is the internal quantum efficiency,

$$\eta_{\text{i}} = \frac{1}{V_{\text{layer}}^{(k)}} \frac{1}{V_{\text{nano}}} \int_{\text{volume}} d\mathbf{r} \int_{\text{layer}} d\mathbf{k}_{\text{f}} p_{\text{em}}(\mathbf{r}, \mathbf{k}_{\text{f}}) \quad (33)$$

In our derivation of eqn (32) and (33), we used eqn (26) and (30). While the electron moves towards the boundary of the nanoparticle, it can experience elastic and inelastic collisions with phonons and cold electrons – finding  $p_{\text{em}}(\mathbf{r}, \mathbf{k}_{\text{f}})$  is quite a complicated physical kinetics problem. References to papers, where various approaches to solve this problem were employed, can be found in ref. 7, 38, 56 and 57. In this paper, we use the simple model, presented in ref. 56, in order to find the probability  $p_{\text{em}}(\mathbf{r}, \mathbf{k}_{\text{f}})$  and to calculate the efficiency  $\eta_{\text{i}}$ . Let us consider first the case where an electron moves to the boundary freely, *i.e.* without collisions. Fig. 5b illustrates this. A hot electron is generated with wave vector  $\mathbf{k}_{\text{f}}$  at point 1 in the sphere at a distance  $r < a$  from its centre (0). The vector  $\mathbf{k}_{\text{f}}$  is directed at an angle  $\theta$  to the axis  $z''$ , which goes from the centre 0 and passes through point 1. Because we assume “collisionless” motion of the electron, it moves along a straight line parallel to the vector  $\mathbf{k}_{\text{f}}$ . The electron collides with the spherical nanoparticle boundary at point 2 with incidence angle  $\alpha$  – see Fig. 5b.

In general, if the electron arrives at the boundary with wave vector  $\mathbf{k}_{\text{s}}$ , the probability  $p_{\text{em}}(\mathbf{r}, \mathbf{k}_{\text{f}})$  is equal to the quantum mechanical (transmission) probability  $t_{\text{bar}}(\mathbf{k}_{\text{s}})$  for this electron to overcome the potential barrier at the boundary between the metal and surrounding medium,  $p_{\text{em}}(\mathbf{r}, \mathbf{k}_{\text{f}}) \equiv t_{\text{bar}}(\mathbf{k}_{\text{s}})$ . The transmission  $t_{\text{bar}}(\mathbf{k}_{\text{s}})$  is a function of the component  $k_{\text{s}}^{(n)}$  of the vector  $\mathbf{k}_{\text{s}}$  normal to the nanoparticle surface at the point of collision between the electron and the surface:  $t_{\text{bar}}(\mathbf{k}_{\text{s}}) \equiv t_{\text{bar}}(k_{\text{s}}^{(n)})$ . It is well-known that the transmission  $t_{\text{bar}}(k_{\text{s}}^{(n)})$  depends strongly on the shape of the potential at the nanoparticle boundary.

In the “collisionless” case of electron motion which we consider at first, the wave vector  $\mathbf{k}_{\text{s}}$  is equal to  $\mathbf{k}_{\text{f}}$ . Therefore,  $k_{\text{s}}^{(n)} = k_{\text{f}} \cos \alpha$  and:

$$p_{\text{em}}^{\text{no coll}}(\mathbf{r}, \mathbf{k}_{\text{f}}) = t_{\text{bar}}(k_{\text{f}} \cos \alpha) \quad (34)$$

In this case, the six-fold integral in (33) can be easily converted into a triple integral:

$$\eta_{\text{i}} = \frac{1}{V_{\text{layer}}^{(k)}} \frac{1}{V_{\text{nano}}} \int_0^a dr 4\pi r^2 \int_{k_{\text{F}}}^{k_{\text{hw}}} dk_{\text{f}} \int_0^\pi d\theta \sin \theta \cdot t_{\text{bar}}(k_{\text{f}} \cos \alpha) \quad (35)$$

where the incidence angle  $\alpha$  is related to the angle  $\theta$  by the theorem of sines:

$$\alpha = \arccos(r \sin \theta / a) \quad (36)$$

The integral in (35) can be calculated analytically for some shapes of the potential – see below.

Now, having considered the simplest collision-free case, we move on to consider a more realistic and more complicated case when the electron can experience collisions during its motion to the surface and is therefore cooled. It is well-known that the dominating mechanism for cooling of hot electrons is their collisions with cold electrons.<sup>58–60</sup> In fact, just one collision of a hot electron with a cold electron renders the hot electron unable to overcome the potential barrier between the metal and surrounding medium. Therefore, in order to calculate the photoelectron emission probability  $p_{\text{em}}(\mathbf{r}, \mathbf{k}_{\text{f}})$  in the case when hot electron collisions are possible, we can simply multiply the “collisionless” probability  $p_{\text{em}}^{\text{no coll}}(\mathbf{r}, \mathbf{k}_{\text{f}})$  [see eqn (34)] by the probability  $P_{\text{t}}(\mathbf{r}, \mathbf{k}_{\text{f}})$  that the hot electron reaches the surface without collisions:

$$p_{\text{em}}(\mathbf{r}, \mathbf{k}_{\text{f}}) = P_{\text{t}}(\mathbf{r}, \mathbf{k}_{\text{f}}) \cdot t_{\text{bar}}(k_{\text{f}} \cos \alpha) \quad (37)$$

Following ref. 56, the probability  $P_{\text{t}}(\mathbf{r}, \mathbf{k}_{\text{f}})$  can be written as

$$P_{\text{t}}(\mathbf{r}, \mathbf{k}_{\text{f}}) = \exp[-L(r, \theta) / l_{\text{e}}(E_{\text{f}})] \quad (38)$$

where

$$L(r, \theta) = \sqrt{a^2 - r^2 \sin^2 \theta} - r \cos \theta \quad (39)$$

is the distance between generation point 1 and point 2 where the electron collides with the nanoparticle surface, as it moves in the metal without collisions (see Fig. 5b); the mean free path  $l_{\text{e}}(E_{\text{f}})$ , generally speaking, depends on the hot electron energy  $E_{\text{f}}$ .<sup>56–60</sup> Correspondingly, from (33) and taking (37) into account, we have:

$$\eta_{\text{i}} = \frac{1}{V_{\text{layer}}^{(k)}} \frac{1}{V_{\text{nano}}} \int_0^a dr 4\pi r^2 \int_{k_{\text{F}}}^{k_{\text{hw}}} dk_{\text{f}} \int_0^\pi d\theta \sin \theta \cdot 2\pi k_{\text{f}}^2 \times \exp[-L(r, \theta) / l_{\text{e}}(E_{\text{f}})] \cdot t_{\text{bar}}(k_{\text{f}} \cos \alpha) \quad (40)$$

Obviously, if  $l_{\text{e}} = \infty$ , eqn (40) coincides with eqn (35).

Using (2), (1), (32) and (25), we can finally express the photoelectron emission cross-section for the volume photoelectric effect through the internal quantum efficiency  $\eta_{\text{i}}$  as:

$$\sigma_{\text{em}}^{\text{volume}} = \frac{8\pi^2}{3} \frac{a}{\lambda_0} \frac{\xi_i''}{\sqrt{\epsilon_e}} |F|^2 \cdot \eta_i a^2 \quad (41)$$

where  $\lambda_0 = 2\pi c/\omega$  is the light wave length in vacuum.

As mentioned above, the probability  $t_{\text{bar}}(k_s^{(n)})$  depends on the shape of the potential  $U(z)$  at the nanoparticle surface. Since we aim to compare surface and volume photoelectric effects, and the surface effect has been calculated above for a step potential (see Fig. 3), we calculate below the internal quantum efficiency  $\eta_i$  firstly for this shape of potential. In this case, the probability  $t_{\text{bar}}$  is:

$$t_{\text{bar}} = \frac{4\text{Re}[s]}{|1+s|^2}, \quad (42)$$

where

$$s = \sqrt{1 - \frac{2mU_b}{\hbar^2(k_s^{(n)})^2}} \equiv \sqrt{1 - \frac{U_b}{E_s^{(n)}}} \quad (43)$$

Fig. 6 illustrates the dependence of the transmission  $t_{\text{bar}}$  on the energy  $E_s^{(n)} = \hbar^2(k_s^{(n)})^2/(2m)$ . When  $E_s^{(n)} > U_b$ , the transmission at first increases sharply and then tends to 1 gradually. On the other hand, many papers (see for instance ref. 7) assume a simpler model dependence:

$$t_{\text{bar}}(E_s^{(n)}) = \begin{cases} 0, & E_s^{(n)} < U_b \\ 1, & E_s^{(n)} > U_b \end{cases} \quad (44)$$

(see the dashed line in Fig. 6), which is a suitable model for a smoothly changing potential (see the dashed green line in Fig. 3) rather than for a sharply changing one. Below we refer to the model in (44) as “model 0-1”.

The thick solid curves in Fig. 7 show the spectral dependence of the internal quantum efficiency  $\eta_i(\hbar\omega)$ , obtained by numerical integration of eqn (40) with the barrier transmission  $t_{\text{bar}}(E_s^{(n)})$  for a step potential [see eqn 42 and 43] and for various radii  $a$  of the spherical nanoparticle: namely  $a = 25$  nm (red line),  $a = 50$  nm (green line), and  $a = 100$  nm (brown line). In

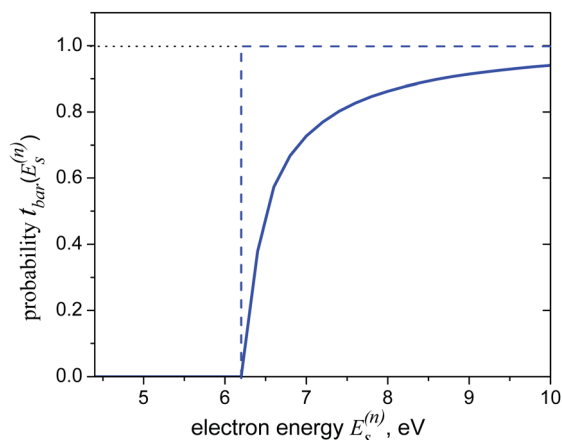


Fig. 6 The (transmission) probability  $t_{\text{bar}}$  for an electron to leave a metal with a step barrier potential with  $U_b = 6.31$  eV as a function of the electron energy  $E_s^{(n)}$ , i.e.  $t_{\text{bar}} = t_{\text{bar}}(E_s^{(n)})$  (solid blue curve). The dashed blue curve shows the probability given by eqn (44) (“model 0-1”).

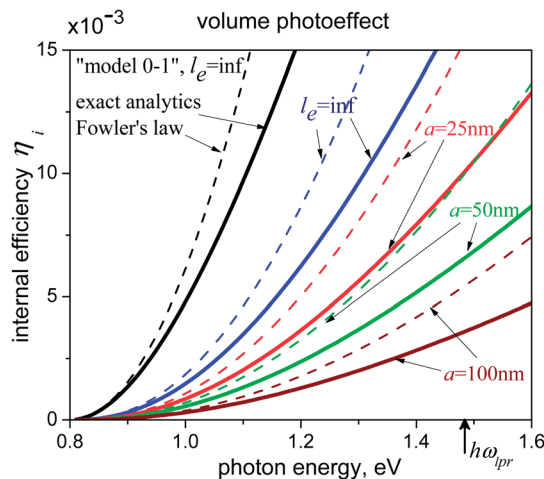


Fig. 7 The spectral dependence of the internal quantum efficiency  $\eta_i(\hbar\omega)$  for the volume photoelectric effect for nanoparticles with different radii  $a$  and different potential shapes at the nanoparticle surface. Red, green and brown solid curves are calculated for  $a = 25$ , 50 and 100 nm, respectively, by numerical integration of eqn (40) for a step potential [see eqn (42) and (43)] and using a mean free path  $l_e = 41$  nm; the dashed curves are obtained using the approximation (45). The blue and black curves are obtained for  $l_e = \infty$  (i.e. for collisionless electron propagation in the nanoparticle) for a step potential and for the ‘model 0-1’ [see eqn (44)], respectively. The blue and black solid lines are exact results given by eqn (40) and (47), respectively, while the blue and black dashed curves are obtained with approximations (45) and (48), respectively.  $\hbar\omega_{\text{pr}}$  is the photon energy at which the plasmonic resonance occurs in the nanoparticle.

the calculations we used the same material parameters for the nanoparticle and the barrier as shown in Fig. 4. For gold, the mean free path  $l_e(E_f)$  changes very weakly, from  $\sim 42$  to  $\sim 40$  nm (ref. 60) for the range of hot electron energies  $E_f$  being considered. Therefore, we have taken the value of  $l_e$  to be constant and used  $l_e = 41$  nm. For comparison, the thick blue line shows the efficiency  $\eta_i$  for the mean free path  $l_e = \infty$ , i.e. for the “collisionless” propagation of hot electrons in a nanoparticle. One sees that electron collisions decrease the efficiency  $\eta_i$  by several times for the shown values of radius  $a$ .

Close to the photoeffect threshold ( $\hbar\omega \rightarrow W_b$ ), one can do the integration in eqn (40) analytically and obtain an approximate formula for the internal efficiency for  $\eta_i$ :

$$\eta_i = F_{\text{st}}(a, l_e) \times \frac{12}{5} \frac{(\epsilon_F + W_b)^{3/2}}{(\epsilon_F + \hbar\omega)^{3/2} - \epsilon_F^{3/2}} \left( \frac{\hbar\omega - W_b}{\epsilon_F + W_b} \right)^{5/2} \quad (45)$$

where

$$F_{\text{st}}(a, l_e) = \frac{l_e}{2a} \left[ 1 - \exp\left(-\frac{2a}{l_e}\right) \right] \quad (46)$$

is the structural function describing the dependence of the efficiency  $\eta_i$  on the nanoparticle size  $a$ . The dependence (45) is illustrated in Fig. 7 by the dashed blue, red, green and brown curves. The parameters used in the calculation of these curves are the same as in the calculations for the solid curves of the same colour. Thus,  $\eta_i \propto (\hbar\omega - W_b)^{5/2}$  close to the threshold – this behaviour coincides with the behaviour of the parameter  $\eta_0$

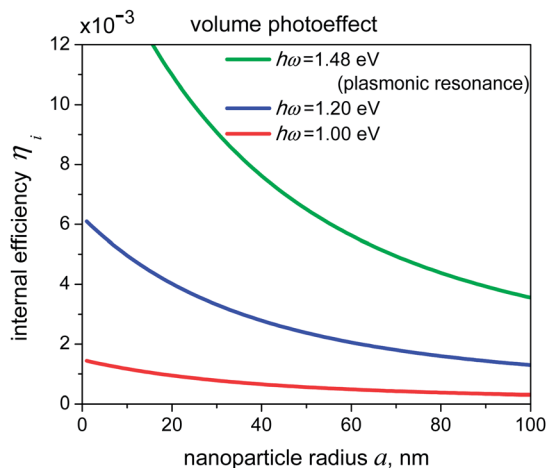


Fig. 8 Dependence of the internal quantum efficiency  $\eta_i$  on the nanoparticle radius  $a$  for three different photon energies:  $\hbar\omega = 1.0, 1.2$  and  $1.48$  eV. The mean free path  $l_e = 41$  nm. The plasmonic resonance takes place in the gold spherical nanoantenna for  $\hbar\omega = 1.48$  eV.

calculated also for the surface effect [see eqn (21) and (22)], with a step potential.

As noted above the model dependence (44) for the transmission  $t_{\text{bar}}(E_s^{(n)})$  is used often. With  $t_{\text{bar}}(E_s^{(n)})$ , the integral in eqn (40) can be calculated analytically for arbitrary excess energy ( $\hbar\omega - W_b$ ) above the photoeffect threshold and is expressed through the exponential integral function  $E_i(z)$  – we do not give the result here due to its bulkiness. But for  $l_e = \infty$  (“collisionless” electron propagation in a nanoparticle) we can derive a simple approximate formula:

$$\eta_i = \frac{(\varepsilon_F + W_b)^{3/2}}{(\varepsilon_F + \hbar\omega)^{3/2} - \varepsilon_F^{3/2}} \left[ \left( \frac{\varepsilon_F + \hbar\omega}{\varepsilon_F + W_b} \right)^{3/2} - \frac{3}{2} \log \frac{\varepsilon_F + \hbar\omega}{\varepsilon_F + W_b} - 1 \right] \quad (47)$$

On the other hand, for arbitrary  $l_e$ , but near the threshold we have the approximation:

$$\eta_i \approx F_{\text{st}}(a, l_e) \times \frac{9}{8} \frac{(\varepsilon_F + W_b)^{3/2}}{(\varepsilon_F + W_b)^{3/2} - \varepsilon_F^{3/2}} \left( \frac{\hbar\omega - W_b}{\varepsilon_F + W_b} \right)^2 \quad (48)$$

These analytic results (47) and (48) for  $l_e = \infty$  are illustrated in Fig. 7 by the black solid and dashed curves, respectively. Obviously, near the photoeffect threshold, eqn (48) yields the parabolic Fowler’s law:  $\eta_i \propto (\hbar\omega - W_b)^2$ . Formulae (47) and (48) with  $l_e = \infty$  are spherical analogues of the corresponding formulae for the internal quantum efficiency for bulk photoelectron emission from thin films which can be found in ref. 7 when electron collisions are neglected.

Fig. 8 shows the dependence of the internal efficiency  $\eta_i$  on the nanoparticle radius  $a$  for different photon energies:  $\hbar\omega = 1.0$  and  $1.2$  eV, and at the plasmonic resonance  $\hbar\omega = \hbar\omega_{\text{pr}} = 1.48$  eV. The behaviour of the curves is described, at least qualitatively, by the structural function (46), and for large  $a$ , the efficiency follows  $\eta_i \propto 1/a$ . This last relationship originates from

the fact that within the quasistatic approximation the photon absorption rate  $R_{\text{abs}}^{\text{volume}}$  is proportional to the nanoparticle volume  $V_{\text{nano}}$  [see eqn (25)] while for large radii  $a \gg l_e$ , the photoelectron emission rate  $R_{\text{em}}^{\text{volume}}$  is proportional to the nanoparticle surface  $A_{\text{nano}}$ . Correspondingly,  $\eta_i \propto A_{\text{nano}}/V_{\text{nano}} \propto 1/a$ . Thus, the behaviour  $\eta_i \propto 1/a$  is a consequence of the fact that the “surface to volume” ratio decreases with increasing nanoparticle size  $a$ . On the other hand, for a smaller radius  $a$  when  $R_{\text{em}}^{\text{volume}} \propto V_{\text{nano}}$ , the efficiency  $\eta_i$  tends to its value in the “collisionless” case – see eqn (35).

### III Comparison of surface and volume mechanisms and discussion

The surface and volume mechanisms for internal photoelectron emission from nanoparticles can be compared by considering the ratio of their photoelectron emission cross-sections:

$$K_{v-s} = \frac{\sigma_{\text{em}}^{\text{volume}}}{\sigma_{\text{em}}^{\text{surface}}} = \frac{2\pi a}{\lambda_0} \frac{\varepsilon_i'' \eta_i}{\eta_0} \quad (49)$$

where we have used eqn (23) and (41) to determine this ratio. Fig. 9 shows the spectral dependence of the ratio  $K_{v-s}(\hbar\omega)$  for different nanoparticle radii:  $a = 100, 50$  and  $25$  nm for the blue, red and brown curves, respectively. The dashed curves are obtained when electron collisions are neglected ( $l_e = \infty$ ), and the solid lines are calculated with  $l_e = 41$  nm.

The dashed curves show that if cooling of hot electrons is absent, the volume photoeffect from nanoparticles can predominate, at least for larger nanoparticles far from the photoeffect threshold. However, if we take into account hot electron cooling during their propagation in a nanoparticle (see solid curves in Fig. 9), we obtain that the surface mechanism is stronger than the volume one throughout almost all of the considered spectrum ranges, and only at  $\hbar\omega > 1.5$  eV does the ratio  $K_{v-s}$  become larger than one. One should note that in the case considered of a gold nanosphere embedded in a medium with  $\varepsilon_e = 13$  the localized plasmonic resonance occurs at  $\hbar\omega \approx \hbar\omega_{\text{pr}} = 1.48$  eV (shown in Fig. 9). Thus, at the plasmonic resonance frequency for the structures considered, the surface and volume mechanisms give comparable contributions to the photoelectron emission rate.

One should stress that the results shown in Fig. 9, and in particular, the dashed curves for “collisionless” electron propagation in the nanoparticle are obtained in the quasistatic approximation,<sup>52</sup> when the electromagnetic field efficiently penetrates into the nanoparticle. In this case, the volume photoelectron emission rate increases proportional to the nanoparticle volume if we neglect electron cooling. On the other hand, the surface photoelectron emission rate increases proportional to the nanoparticle surface area. Correspondingly, if we neglect the electron collisions, the growing role of the volume mechanism with increasing nanoparticle sizes can be attributed to the quasistatic approximation. In fact, this approximation works only for relatively small plasmonic nanoparticles, and already for  $a = 100$  nm the field penetrates into the nanoparticle volume only partially.<sup>52</sup> Thus, the model

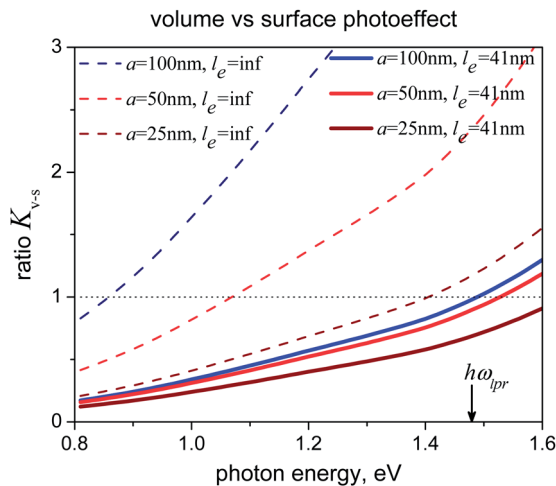


Fig. 9 Spectral dependence on the ratio  $K_{v-s} = \sigma_{\text{em}}^{\text{volume}}/\sigma_{\text{em}}^{\text{surface}}$  for various values of the nanoparticle radius  $a$  and the mean free path  $l_e$ . For the plasmonic resonance,  $\hbar\omega \approx \hbar\omega_{\text{ipr}} = 1.48 \text{ eV}$ .

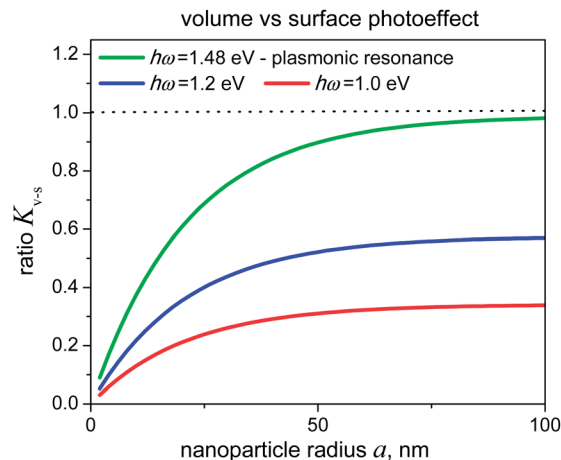


Fig. 10 Dependence of the ratio  $K_{v-s} = \sigma_{\text{em}}^{\text{volume}}/\sigma_{\text{em}}^{\text{surface}}$  on the nanoparticle radius  $a$  for three different photon energies:  $\hbar\omega = 1.0, 1.2$  and  $1.48 \text{ eV}$ . The mean free path  $l_e = 41 \text{ nm}$ .

used here can seriously overestimate the volume mechanism for large nanoparticles if we neglect the hot electron cooling, as shown by the dashed curves in Fig. 9.

Fig. 10 shows the ratio  $K_{v-s}$  as a function of the nanoparticle radius  $a$  for different photon energies:  $\hbar\omega = 1.0, 1.2 \text{ eV}$  and for the case of plasmonic resonance  $\hbar\omega = \hbar\omega_{\text{ipr}} = 1.48 \text{ eV}$ . One sees that the ratio  $K_{v-s}$  tends to zero with decreasing radius  $a$ . Such a behaviour again results from the scaling of the “surface to volume” ratio at small  $a$ . Namely, for  $a \ll l_e$  the volume photoelectron emission rate is  $R_{\text{em}}^{\text{volume}} \propto V_{\text{nano}}$ , while the surface photoelectron emission rate is  $R_{\text{em}}^{\text{surface}} \propto A_{\text{nano}}$ . Therefore,  $K_{v-s} = R_{\text{em}}^{\text{volume}}/R_{\text{em}}^{\text{surface}} \propto V_{\text{nano}}/A_{\text{nano}} \propto a$ . On the other hand, one sees from Fig. 10 that for larger values of the radius  $a$  ( $a \gg l_e$ ) when the hot electrons generated far from the surface cannot reach it due to cooling by collisions, both the rates  $R_{\text{em}}^{\text{volume}}$  and  $R_{\text{em}}^{\text{surface}}$  become proportional to the nanoparticle surface area  $A_{\text{nano}}$ , and correspondingly, the ratio  $K_{v-s}$  does not change with the radius  $a$  any more.

Now we would like to discuss the assumptions made in the calculation of the volume mechanism in more detail. The first one is the quasistatic approximation, which leads to an overestimation of the volume effect for larger nanoparticles, as discussed above. Another assumption concerns the distribution of hot electrons in  $k$ -space – see eqn (30) and (31). In fact, we ascribe the light absorption, which is defined by the experimentally measured value of the imaginary part  $\epsilon_2''(\omega)$  of the metal relative permittivity, uniformly to all possible optical transitions from the states under the Fermi level; as a result, the hot electrons populate the volume in  $k$ -space, given by eqn (27), equally. This means that the dependence of the hot electron distribution on the energy  $E_f$  is proportional to  $\sqrt{E_f}$ . On the other hand, Chen and Bates<sup>56</sup> considered that the distribution is proportional to the “joint density of states” which is  $\propto \sqrt{E_f(E_f - \hbar\omega)}$ . Our analysis shows that use of the latter distribution instead of the Fowler’s one can increase the volume effect but only slightly – by 2–7%.

Furthermore, it is well-known that optical transitions from deeper states under the Fermi level can contribute to the optical absorption more strongly than the transitions from states that lie closer to the Fermi level.<sup>38,61</sup> It is clear that transitions from deeper levels populate states above the Fermi level with lower energies than is the case for transitions from less deep levels. Hence, lower-energy states above the Fermi level are populated with hot electrons more strongly than the higher-energy levels; it is only from these latter levels that electron emission from the metal is in principle possible. In other words, transitions from deeper levels can contribute strongly to light absorption in metals but not to photoelectron emission, since such transitions do not generate hot electrons of sufficient energy so as to overcome the barrier. Thus, the assumption of a homogeneous population (30) of the layer (27) (the assumption by Fowler) can lead, generally speaking, to an overestimation of the internal quantum efficiency  $\eta_i$  for the volume mechanism. This can particularly impact the metal interband transitions.<sup>61</sup> Note that the realisation that optical transitions of electrons in the bulk can determine the optical absorption of a metal, but are unable to provide photoelectron emission, was one of the basic ideas of the paper by Tamm and Schubin.<sup>36</sup> However, these strong transitions from deeper energy levels in gold appear to become substantial only at photon energies higher than  $\sim 1.5\text{--}2 \text{ eV}$ ,<sup>54,61</sup> so that for the photon energy range under consideration (*i.e.*  $\hbar\omega < 1.6 \text{ eV}$ ) the assumption of uniform population of states by hot electrons looks rather reasonable.

On the other hand, the model (37)–(39) for hot electron cooling due to collisions with cold electrons can underestimate the electron cooling rate. Indeed, the model neglects, in some sense, the role of elastic collisions of the hot electron. Such collisions do not affect the hot electron energy directly, but can make the electron path in the nanoparticle longer than the straight line (39), which can lead to a stronger electron cooling.

Nevertheless, despite the limitations brought about by the above assumptions, we can suggest that it appears unlikely that more precise models would significantly alter the conclusion

that we draw from the calculations in this work, namely, that the cooling of hot electrons leads to a serious decrease of the photoelectron emission rate due to the volume mechanism. Together with the fact that the surface mechanism of the photoelectric effect does not suffer from electron collisions in the bulk at all, this lets us conclude that the surface mechanism prevails over the volume one in plasmonic nanoantennas for the majority of considered conditions.

Let us finally recall that the case when the surface and volume mechanisms appear to be comparable to each other, *i.e.*, under the plasmonic resonance conditions (see Fig. 9 and 10), is obtained here for spherical nanoparticles. It is well known that the plasmonic resonance in oblate spheroids, which are good models for nanoparticles in many experimental configurations, is red-shifted if incident light is polarized along the longer axis.<sup>6,52</sup> In accordance with Fig. 9, one could assume that in such nanoantennas the surface photoelectric effect can prevail also in the case of plasmonic resonance. Numerical calculations of photoelectron emission from nanoparticles with shapes more complicated than spherical, as well as from ensembles of nanoparticles, are the subject of forthcoming planned studies.

## IV Conclusion

We have carried out calculations of internal photoelectron emission from plasmonic nanoparticles into a surrounding semiconductor matrix for the IR range of photon energies for two mechanisms of the effect – surface and volume ones. We have shown that the surface photoeffect would prevail over the volume one in the case of internal photoelectric effect from small nanoparticles, which extends the initial conclusion made by Tamm and Schubin in 1931 from a single flat interface to nanostructures. From our calculations, this predominance of the surface effect is a result of the effective cooling of hot carriers generated by the volume mechanism during their propagation from the inside of the nanoparticle to its surface. Calculations have been carried out for a step potential at the nanoparticle surface, and a simple model for the hot electron cooling has been used. Nevertheless, it is unlikely that these model limitations would change the overall conclusion. To our knowledge such a comparison of the two mechanisms for the photoeffect from plasmonic nanoparticles has been undertaken here for the first time.

We also stress the important effect of the discontinuity of the dielectric permittivity at the nanoparticle boundary in the surface mechanism, which leads to a substantial (by  $\sim 5$  times) increase in the photoelectron emission rate from a nanoparticle compared to the case when such a discontinuity is absent.

Confidence in the predominance of the surface mechanism can be useful in the design of devices based on the photoelectric effect and on the use of hot electrons from plasmonic nanoantennas. In particular, it is clear that the angular pattern of photoelectrons can be different for the surface and volume photoeffect. For instance, for spherical nanoparticles, in the case of the volume mechanism electrons are emitted in all directions equally, while in the case of the surface one, electrons

are emitted mainly in a direction parallel to the electric field polarization of the incident light, because the photoelectron emission rate in the surface mechanism is proportional to the square of the electric field component normal to the nanoparticle surface. Correspondingly, parts of a nanoantenna surface where the normal component is maximal must have good contact with the surrounding matrix in order for efficient electron emission to occur. It appears that this circumstance played a key role in ref. 12, where a substantial increase of the responsivity of the device was reached by proper embedding of the nanoantennas into the semiconductor substrate.

## Acknowledgements

A.V.U. and I.E.P. acknowledge financial support from the Russian Foundation for Basic Research (Project no. 14-02-00125) and the Russian MSE State Contract N14.527.11.0002 and support from the CASE project (Denmark). V.E.B. acknowledges financial support from SPIE Optics and Photonics Education Scholarship, as well as Otto Mønstedts and Kaj og Hermilla Ostenfeld foundations. S.V.Z. acknowledges financial support from the People Programme (Marie Curie Actions) of the European Union's 7th Framework Programme FP7-PEOPLE-2011-IIF under REA grant agreement no. 302009 (Project HyPHONE). E.P.O'R. acknowledges support from Science Foundation Ireland (project no. 06/IN.1/I90).

## References

- 1 H. Chalabi and M. L. Brongersma, *Nat. Nanotechnol.*, 2013, **8**, 229.
- 2 Y. Nishijima, K. Ueno, Y. Yokota, K. Murakoshi and H. Misawa, *J. Phys. Chem. Lett.*, 2010, **1**, 2031.
- 3 M. W. Knight, H. Sobhani, P. Nordlander and N. J. Halas, *Science*, 2011, **332**, 702.
- 4 Y. Takahashi and T. Tatsuma, *Appl. Phys. Lett.*, 2011, **99**, 182110.
- 5 Y. K. Lee, C. Ho Jung, J. Park, H. Seo, G. A. Somorjai and J. Y. Park, *Nano Lett.*, 2011, **11**, 4251.
- 6 I. E. Protsenko and A. V. Uskov, *Phys.-Usp.*, 2012, **55**, 508.
- 7 C. Scales and P. Berini, *IEEE J. Quantum Electron.*, 2010, **46**, 633.
- 8 A. Akbari and P. Berini, *Appl. Phys. Lett.*, 2009, **95**, 021104.
- 9 P. Berini, *Laser Photonics Rev.*, 2014, **8**, 197.
- 10 I. Goykhman, B. Desiatov, J. Khurgin, J. Shappir and U. Levy, *Nano Lett.*, 2011, **11**, 2219.
- 11 A. Novitsky, A. V. Uskov, C. Gritti, I. E. Protsenko, B. E. Kardynał and A. V. Lavrinenko, *Prog. Photovolt.: Res. Appl.*, 2014, **22**, 422.
- 12 M. W. Knight, Y. Wang, A. S. Urban, A. Sobhani, B. Y. Zheng, P. Nordlander and N. J. Halas, *Nano Lett.*, 2013, **13**, 1687.
- 13 A. Sobhani, M. W. Knight, Y. Wang, B. Zheng, N. S. King, L. V. Brown, Z. Fang, P. Nordlander and N. J. Halas, *Nat. Commun.*, 2013, **4**, 1643.
- 14 S. V. Zhukovsky, V. E. Babicheva, A. V. Uskov, I. E. Protsenko and A. V. Lavrinenko, *Plasmonics*, 2013, DOI: 10.1007/s11468-013-9621-z.

- 15 S. V. Zhukovsky, V. E. Babicheva, A. B. Evlyukhin, I. E. Protsenko, A. V. Lavrinenko and A. V. Uskov, Photogalvanic Effect in Plasmonic Non-Centrosymmetric Nanoparticles, <http://arxiv.org/abs/1312.2428>.
- 16 E. A. Moulin, U. W. Paetzold, B. E. Pieters, W. Reetz and R. Carius, *J. Appl. Phys.*, 2013, **113**, 144501.
- 17 T. P. White and K. R. Catchpole, *Appl. Phys. Lett.*, 2012, **101**, 073905.
- 18 F. Wang and N. A. Melosh, *Nano Lett.*, 2011, **11**, 5426.
- 19 A. K. Pradhan, T. Holloway, R. Mundle, H. Dondapati and M. Bahoura, *Appl. Phys. Lett.*, 2012, **100**, 061127.
- 20 F. P. Garcia de Arquer, A. Mihi, D. Kufer and G. Konstantatos, *ACS Nano*, 2013, **7**, 3581.
- 21 F. B. Atar, E. Battal, L. E. Aygun, B. Daglar, M. Bayindir and A. K. Okyay, *Opt. Express*, 2013, **21**, 7196.
- 22 M. Grätzel, *Nature*, 2001, **414**, 338.
- 23 E. W. McFarland and J. Tang, *Nature*, 2003, **421**, 616.
- 24 J. R. Renzas and G. A. Somorjai, *J. Phys. Chem. C*, 2010, **114**, 17660.
- 25 Y. Li and G. A. Somorjai, *Nano Lett.*, 2010, **10**, 2289.
- 26 I. Thomann, B. A. Pinaud, Z. Chen, B. M. Clemens, Th. F. Jaramillo and M. L. Brongersma, *Nano Lett.*, 2011, **11**, 3440.
- 27 S. Mukherjee, F. Libisch, N. Large, O. Neumann, L. V. Brown, J. Cheng, J. B. Lassiter, E. A. Carter, P. Nordlander and N. J. Halas, *Nano Lett.*, 2012, **13**, 240.
- 28 S. C. Warren and E. Thimsen, *Energy Environ. Sci.*, 2012, **5**, 5133.
- 29 S. Mubeen, J. Lee, N. Singh, S. Krämer, G. D. Stucky and M. Moskovits, *Nat. Nanotechnol.*, 2013, **8**, 247.
- 30 M. Xiao, R. Jiang, F. Wang, C. Fang, J. Wang and J. C. Yu, *J. Mater. Chem. A*, 2013, **1**, 5790.
- 31 D. Conklin, S. Nanayakkara, T.-H. Park, M. F. Lagadec, J. T. Stecher, X. C. Chen, M. J. Therien and D. A. Bonnell, *ACS Nano*, 2013, **7**, 4479.
- 32 J. W. Schwede, I. Bargatin, D. C. Riley, B. E. Hardin, S. J. Rosenthal, Y. Sun, F. Schmitt, P. Pianetta, R. Howe, Z.-X. Shen and N. A. Melosh, *Nat. Mater.*, 2010, **9**, 762.
- 33 C. Ropers, T. Elsaesser, G. Giulio Cerullo, M. Zavelani-Rossi and C. Lienau, *New J. Phys.*, 2007, **9**, 397.
- 34 F.-J. Meyer zu Heringdorf, L. I. Chelaru, S. Möllenbeck, D. Thien and M. Horn-von Hoegen, *Surf. Sci.*, 2007, **601**, 4700.
- 35 M. I. Stockman, M. F. Kling, U. Kleineberg and F. Krausz, *Nat. Photonics*, 2007, **1**, 539.
- 36 I. Tamm and S. Schubin, *Z. Phys.*, 1931, **68**, 97.
- 37 U. Kreibig and M. Vollmer, *Optical Properties of Metal Clusters*, Springer-Verlag, Berlin Heidelberg, 1995.
- 38 N. V. Smith, *CRC Crit. Rev. Solid State Sci.*, 1971, **2**, 45.
- 39 C. Kittel, *Quantum Theory of Solids*, John Wiley & Sons, 2nd edn, 1989.
- 40 J. M. Ziman, *Principles of the Theory of Solids*, Cambridge University Press, 2nd edn, 1972.
- 41 K. Mitchell, *Proc. R. Soc. London, Ser. A*, 1934, **146**, 442.
- 42 R. E. B. Makinson, *Phys. Rev.*, 1949, **75**, 1908.
- 43 A. M. Brodsky and Y. Y. Gurevich, *Sov. Phys. JETP*, 1968, **27**, 114.
- 44 A. M. Brodsky, Y. Y. Gurevich and V. G. Levich, *Phys. Status Solidi*, 1970, **40**, 139.
- 45 A. M. Brodsky and Y. Y. Gurevich, *Theory of Electron Emission from Metals*, Nauka, Moscow, 1973.
- 46 J. G. Endriz and W. E. Spicer, *Phys. Rev. Lett.*, 1971, **27**, 570.
- 47 J. G. Endriz, Photoemission studies of surface-plasmon oscillations on controlled-roughness aluminum films, Ph.D. thesis, Stanford University, 1970.
- 48 J. G. Endriz, *Phys. Rev. B: Solid State*, 1973, **7**, 3464.
- 49 A. A. Maradudin and D. L. Mills, *Phys. Rev. B: Solid State*, 1975, **11**, 1392.
- 50 H. Petersen, *Z. Physik B*, 1978, **31**, 171.
- 51 A. O. Govorov, H. Zhang and Y. K. Gun'ko, *J. Phys. Chem. C*, 2013, **117**, 16616.
- 52 S. A. Maier, *Plasmonics: Fundamentals and Applications*, Springer Science+Business Media LLC, 2007.
- 53 V. L. Ginzburg and I. M. Frank, *J. Exp. Theor. Phys.*, 1946, **16**, 15.
- 54 M. J. Weber and J. Marvin, *Handbook of optical materials*, CRC Press LLC, 2003.
- 55 R. H. Fowler, *Phys. Rev.*, 1931, **38**, 45.
- 56 Q. Y. Chen and C. W. Bates, *Phys. Rev. Lett.*, 1986, **57**, 2737.
- 57 C. N. Berglund and W. E. Spicer, *Phys. Rev.*, 1964, **136**, 1030.
- 58 R. Stuart, F. Wooten and W. E. Spicer, *Phys. Rev.*, 1964, **135**, 495.
- 59 J. J. Quinn, *Phys. Rev.*, 1962, **126**, 1453.
- 60 K. W. Frese and C. Chen, *J. Electrochem. Soc.*, 1992, **139**, 3234.
- 61 G. V. Hartland, *Chem. Rev.*, 2011, **111**, 3858.